LA-UR-17-28604

Title:	Quantification of uncertainty in photon source spot size inference during laser-driven radiography experiments at TRIDENT
Author(s):	Tobias, Benjamin John; Palaniyappan, Sasikumar; Gautier, Donald Cort; Mendez, Jacob; Burris-Mog, Trevor John; Huang, Chengkun; Favalli, Andrea; Hunter, James F.; Espy, Michelle A.; Schmidt, Derek William; Nelson, Ronald Owen; Sefkow, Adam; Shimada, Tsutomu; Johnson, Randall Philip; Fernandez, Juan Carlos
Intended for:	Report
Issued:	2019-01-22 (rev.2)

Quantification of uncertainty in photon source spot size inference during laser-driven radiography experiments at TRIDENT

Benjamin John Tobias*,[1], S. Palaniyappan[1], D.C. Gautier[1], J. Mendez[1], T. Burris[1], C.K. Huang[1], A. Favalli[1], J.F. Hunter[1], M.E. Espy[1], D.W. Schmidt[1], R.O. Nelson[1], A. Sefkow[2], T. Shimada[1], R.P. Johnson[1], J.C. Fernandez[1]

[1]*Los Alamos National Laboratory, New Mexico 87545*
[2]*University of Rochester, New York 14627*

**e-mail* tobias@lanl.gov

Images of the R2DTO resolution target were obtained during laser-driven-radiography experiments performed at the TRIDENT laser facility, and analysis of these images using the Bayesian Inference Engine (BIE) determines a most probable full-width half maximum (FWHM) spot size of 78 μm. However, significant uncertainty prevails due to variation in the measured detector blur. Propagating this uncertainty in detector blur through the forward model results in an interval of probabilistic ambiguity spanning approximately 35-195 μm when the laser energy impinges on a thick (1 mm) tantalum target. In other phases of the experiment, laser energy is deposited on a thin (~100 nm) aluminum target placed 250 μm ahead of the tantalum converter. When the energetic electron beam is generated in this manner, upstream from the bremsstrahlung converter, the inferred spot size shifts to a range of much larger values, approximately 270-600 μm FWHM. This report discusses methods applied to obtain these intervals as well as concepts necessary for interpreting the result within a context of probabilistic quantitative inference.

I. INTRODUCTION

Quantitative uncertainty analysis is a critical aspect of data reduction and inference from experimental observation. In comparison to sensitivity analysis [Bode 1945, Wigner 1945], which aims to understand how the variation of an outcome depends on the variation of independent variables, quantification of the uncertainty inherent to inference of the independent variables allows one to develop definitive metrics for given experiments and instrumentation, even develop methods for increasing the precision of new data [Rabinovich 2000, Ronen 1988]. This is of the utmost importance, for example, in qualifying experimental design for compliance with measurement specifications. This paper describes methods applicable to quantitatively determining uncertainty by comparison of a single radiographic image of a 2D resolution target to an inherently imperfect synthetic diagnostic model. The inferences made by this comparison, as will be discussed, are dependent upon the quality of the model and the quality of prior information about input parameters.

Quantitative discussions of the reliability of an inference are often subject to the choice of metric. To wit, so long as the fitting metric, or appropriately defined χ^2, is monotonic and well-behaved around a single optimum solution, a single most probable solution exists and it is possible to portray all other solutions as less likely by some degree [Laplace 1774, 1814]. One may encapsulate uncertainty with a confidence interval, or a region over which the single-valued posterior probability varies within given limits [BIPM 2008]. However, the threshold that defines these limits (e.g. 68% confidence, 95% confidence, etc.) is chosen in a rather arbitrary manner. That arbitrariness is avoided in this work by ignoring less likely solutions--no attempt is made to directly evaluate the probability of a given solution or to evaluate the change in probability relative to an optimal solution. Instead, uncertainty is quantified by recognizing that some parameters of the model cannot be simultaneously optimized, but are defined a priori, either through external experiments or independent measurement, and carry with them some inherent uncertainty that must be propagated through the analysis until it imparts, effectively, an error bar on the probability of values assigned to other independent variables. By way of propagating errors (or in some contexts the convolution of probability distribution functions), the fitting metric may become decidedly less well-behaved. It is this choice of paradigm, the situation in which multiple values of χ^2 correspond to the same set of independent variables, and likewise multiple solutions with equal probability may co-exist, that an unambiguous interval of uncertainty in the quantity of interest can be established.

The uncertainty analysis developed in Sections II and III is applied in Section IV to the inference of radiographic spot size from resolution target imaging data. This application provides an example of the analysis algorithm in a relatively simple situation having a minimal number of assumptions and free parameters that are easily classified as either variables of interest or parameters taken from prior knowledge. Furthermore, many of the secondary variables exhibit no covariance with the primary variable of interest in their impact on χ^2 and can be fit independently. For example, within the analysis model, the definition of the photon energy spectrum has no bearing on the blurring of the image. These and other important approximations that are validated by inspection of the data allow the analysis to be carried out efficiently and in a manner that emphasizes the most important, most basic, aspects of the uncertainty model.

For the discussion that follows, it is assumed that the fitting error metric is well-behaved and that a single optimal maximum likelihood solution exists within the parameter space of interest. If these assumptions are violated, then the significance of these findings is limited to the resolution of a local minimum in the value of χ^2. This analysis does not address the inherent uncertainty associated with the question as to whether other local minima exist.

II. ERROR ANALYSIS AND OPTIMIZATION

The analysis performed using the BIE [Hanson 1993, Hanson and Cunningham 1996] compares a single radiographic image obtained in experiment with a synthetic image produced by forward modeling. The fit to the data is evaluated by computing a standard χ^2 error metric that sums the discrepancy of the i^{th} pixel over all N pixels. This figure of merit consists of three components: a *model parameter error* that encapsulates differences between the state of the model at the current iteration step and the optimal state that will be obtained when all parameters of the model are optimized, a *random error* that results from stochastic processes producing noise in the experimental data, and a *systematic error* that may be attributed to inadequacies of the model. If the random processes are assumed to be Gaussian, then this may be expressed by the following equation:

$$\chi^2 = \sum_{i=1}^{N}([M_i(\boldsymbol{a},\boldsymbol{b}) - M_i(\boldsymbol{a_0},\boldsymbol{b_0})] + \sigma_i + \varphi_i)^2, \tag{1}$$

where the integer ***i*** refers to an individual data point amongst N data points, M_i refers to the modeled data, vectors $\boldsymbol{a}$ and $\boldsymbol{b}$ contain the model parameters and the independent variables to be inferred, respectively, σ_i is the i^{th} realization of the random process with Gaussian distribution, and φ represents all errors that are not accounted for by well-modeled effects or zero-mean stochastic processes. If the forward model is properly optimized, the minimum χ^2 that results is the sum of contributions from random and systematic errors only. Note that this χ^2 is defined in accordance with its use in a least-squares fitting approach to model optimization; in the example problem presented later, the BIE is operated in a least-squares fitting mode of optimization. Were one to begin their analysis using the method of maximum likelihood, alternative definitions of χ^2 would be possible for which the variance associated with stochastic processes may appear as a weighting denominator [Bevington 1969]. This is discussed further in Section V.

For a small number of data points, N, random errors may cause the value of χ^2 to vary unpredictably as the inputs to the forward model, $\boldsymbol{a}$ and $\boldsymbol{b}$, are varied. Noise in a single pixel may add to or cancel a localized error induced by variation of an input parameter. However, if the impact of varying a given input parameter is not highly localized within the image, then for large values of N the random error term reduces to a constant, $N\sigma^2$ for a Gaussian probability distribution, appearing outside the summation:

$$\chi^2 = \sum_{i=1}^{N}[M_i(\boldsymbol{a},\boldsymbol{b}) - M_i(\boldsymbol{a_0},\boldsymbol{b_0})]^2 + N\sigma^2 + \Phi^2. \tag{2}$$

In this limit, comparison of the least-squares fitting data to the contribution from random noise, i.e.,

$$\Phi^2(\boldsymbol{a},\boldsymbol{b}) = \chi^2 - \sum_{i=1}^{N}[M_i(\boldsymbol{a},\boldsymbol{b}) - M_i(\boldsymbol{a_0},\boldsymbol{b_0})]^2 - N\sigma^2, \tag{3}$$

can reveal the relative importance and dependent behavior of the accumulated systematic errors, $\Phi^2 = \sum_{i=1}^{N}(\phi_i^2 + 2M_i\phi_i)$. This is illustrated in Figure 1. The model error term, $\sum_{i=1}^{N}[M_i(\boldsymbol{a},\boldsymbol{b}) - M_i(\boldsymbol{a_0},\boldsymbol{b_0})]^2$, can be evaluated externally, and empirical statements about the adequacy of the model, M, can be made. If the model properly represents the physics of the measurement (and assumptions of separability noted above are valid), then one should expect a vanishingly small contribution from the systematic error term, Φ^2, and a contribution from random errors that is independent of $\boldsymbol{a}$ and $\boldsymbol{b}$.

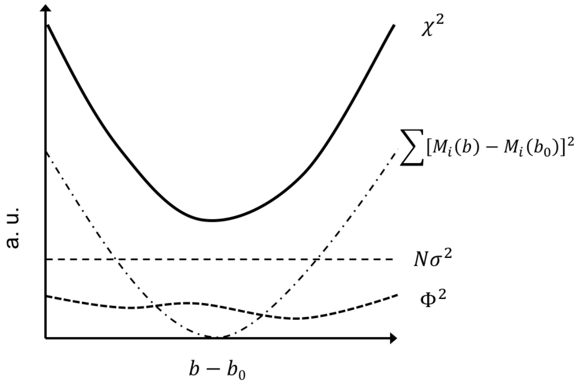

Figure 1. *Illustrative representation of the terms described in Equation (2). The total* χ^2 *is the sum of a well-behaved and well-understood error in the optimization of the forward model, an asymptotically converged term encompassing all random, stochastic processes, and a term encompassing all systematic errors that are not accounted for by the model and that may be dependent on variation of model parameters.*

In the analysis discussed so far, the synthetic diagnostic forward model produces a synthetic image, M, as a function of input vectors $\boldsymbol{a}$ and $\boldsymbol{b}$. These two input vectors are distinguished as containing either *model parameters*, a_j, that are determined by external means and to which prior probability distributions may be assigned, or as *optimizable variables*, b_k. The latter may correspond either to unknown quantities that are simply unimportant to the experimental objectives, i.e. fitting parameters such as those describing the alignment of the image in the analysis grid, or to quantities of interest that are to be inferred from the analysis. If there are m parameters a_j and n parameters b_k, then χ^2 is single-valued at all points within a space having dimensions $m+n$. Treating all a_j and b_k as independent variables and optimizing along all of these axes would result in a least-squares fit that corresponds to the maximum likelihood solution for a single image. However, it becomes difficult to quantify the certainty of that solution in unambiguous terms. Ignoring the possibility of a dead band in the measurement apparatus or degenerate solutions, χ^2 is larger at all points $\{\boldsymbol{a} \neq \boldsymbol{a}_0 \cup \boldsymbol{b} \neq \boldsymbol{b}_0\}$ around the optimal solution. Evaluation of the directional gradients along a principle curvature of this space reveals the sensitivity of the model on input parameters [Myers 1971, Hanson and Cunningham 1994], but it takes on quantitative meaning only in relation to another model, different data, or statistical fluctuations. It provides no definitive quantitative interval of uncertainty in the inference of a single parameter: the maximum likelihood solution is the most probable and any chosen threshold in the change of χ^2 that would define a confidence interval is arbitrary. However, we may reduce the dimensionality of the χ^2 surface to the n dimensions corresponding to the *optimizable variables*, b_k, by considering the *model parameters*, a_j, separately. They are each associated with prior probability distributions, $P(a_j)$, that propagate through the model to produce error bars on χ^2 [Shapiro and Gross 1981, Ronen 1988, Cowen 1998, Rabinovich 2000]. The prior probability distribution $P(a_j)$ is not regarded as a range that *may* be considered, but rather as a range that *must* be considered, and an increase in χ^2 does not justify dismissal of a value for a_j as it would the rejection of a solution b_k. This allows one to quantify an interval of uncertainty as a function of the curvature of the fitting metric, $\frac{\partial^2}{\partial \boldsymbol{b}_k^2}\chi^2$, and the height of an error bar that corresponds to the nested probability distribution, $P(\chi^2|P(\boldsymbol{a}))$.

III. UNCERTAINTY ANALYSIS

In this paper, the *uncertainty interval* is defined as the largest contiguous region of parameter space about an inferred quantity of interest, within the domain of the assigned prior probability distribution functions, where equal values of the least-squares fitting error may be obtained. The first step toward obtaining this interval is the construction of a synthetic diagnostic forward model that generates synthetic image data from the known experimental conditions and the researcher's understanding of physical processes utilized by the instrumentation. Here, this is realized in the form of a BIE canvas that manipulates both the data and a simplified model of photon transport through the radiographic target. Typical manipulations in this canvas include: 2D scaling (effective variation of radiographic magnification); shifting within the 2D plane and rotating of the image data (with interpolation onto a uniform grid); definition of convolution kernels representing sources of image blur; multiplicative gain modification; and modulation of an additive field representing scattered radiation. The photon spectrum may also be manipulated, but within this simplified model those changes impact only the direct photon transport and can be compensated for with multiplicative and/or additive fields without requiring re-optimization of the image blur kernels. The quantity of interest in the application example to be discussed here is the radiographic source blur kernel, or equivalently the radiographic spot size. An algorithm for identifying the most likely spot size, and an uncertainty interval about this solution, by classifying the available manipulations and resultant χ^2 data is described in terms of the framework introduced in Section II above.

Within the BIE canvas, the *optimizable variables*, those parameters to which one assigns no prior knowledge (within reasonable limits), include the degree of image scale, shift, and rotation required to geometrically align the data and the model. These geometric manipulations are, in general, independent of other manipulations of the canvas and therefore do not need to be re-optimized subsequent to changing the value of other parameters (except as periodic verification of the initial image re-orientation). Other optimizable variables include the parameterization of multiplicative and additive fields that represent the effects of detector gain and photon scatter (these manipulations tend to absorb errors in the definition of the photon spectrum and target thickness). Each of the optimizable variables described thus far can be adjusted with great freedom to best fit the data. A single optimizable variable, the resolving power of the source blur kernel, or the inferred spot size, is identified as the quantity of interest. This parameter will be the principle axis of the subsequent uncertainty analysis.

The most important *model parameter*, a quantity to which one assigns a prior probability distribution function based on the outcome of separate analysis, is the resolving power of the detector, i.e. the detector blur function. For the given experiment, phosphor image plates [Sayag 2004, Seely 2008] are stacked between sheets of tantalum intensifier material. Estimates of the blur function for this arrangement have been developed previously, with the best-case resolving power found to have a cutoff frequency of 0.59 lp/mm. The resolving power of the specific image plates used throughout the experiment was obtained by analyzing images of the resolution target at a radiographic magnification of unity, i.e. the resolution target was placed in direct contact with the image plate, on location at the TRIDENT laser facility. Analysis of 4 image plates exposed simultaneously during a single laser discharge, resulted in a range of values from 0.3 to 0.4 lp/mm. A reasonable prior probability distribution function for this limited data is then a rectangular function with these limits. (Note: under-estimating the resolving power of the detector image plates will correspond with under-estimating the source spot size. Therefore, substituting 0.59 lp/mm for the values obtained during the laser experiment would result in a larger estimate for the source full width at half maximum metric.)

When all applicable approximations hold, the above model and definitions dictate the following algorithm for determining the maximum likelihood solution and uncertainty interval for the source spot size:

1- Using established best practices for the BIE [Disterhaupt 2015], all *optimizable variables* and *model parameters* are optimized to obtain the best least-squares fit to the data. In the example problem, this is done for each laser discharge, each image plate, and each pre-selected functional form of the source spot size. Given that all optimized values lie within their physically allowable ranges, or prior probability distribution functions, the optimal point corresponds to the maximum likelihood solution, $(\boldsymbol{a}_0, \boldsymbol{b}_0)$. Furthermore, the value $\chi^2(\boldsymbol{a}_0, \boldsymbol{b}_0)$ obtained here may be related, with certain caveats discussed in Section V, to the inverse logarithm of the solution's posterior probability [Bevington 1969].
2- All *model parameters* are varied across the extent of their prior probability distributions so as to establish an upper bound on the value of χ^2 for the best *optimization parameters*. The maximum value of χ^2 found in this step is identified and recorded as $\chi^2_{max}(\boldsymbol{b}_0)$.
3- The *optimization parameter of interest*, b_1, is forced away from its optimized value, $b_{1,0}$. This step re-centers the analysis at a new point on the principle axis, $x = b - b_0$, and provides the value $\chi^2(\boldsymbol{a}_0, \boldsymbol{b})$.
4- All other *optimizable variables*, b_k, are optimized while keeping the optimization parameter of interest, b_1, fixed. This ensures that one remains on a principle curvature of the multi-dimensional surface $\chi^2(\boldsymbol{a}_0, \boldsymbol{b})$. In other words, one translates in the optimization parameter space along the direction of slowest ascent.
5- The *model parameters* are again varied across their prior probability distributions to generate error bars. In practice, this requires optimization of the *model parameters*, $\boldsymbol{a}$, to locate the lower extent of the error bar, $\chi^2_{min}(\boldsymbol{b})$. The upper extent of the error bar may correspond to either limit of the prior probability distribution for a. (Note: this step requires, in general, a multi-dimensional optimization. However, the given task is simplified by the fact that there is only a single model parameter, the detector blur kernel.)
6- For simplicity at this step, consider the situation illustrated in Figure 2. The value of $\chi^2_{min}(\boldsymbol{b})$ is compared to $\chi^2_{max}(\boldsymbol{b}_0)$. If $\chi^2_{min}(\boldsymbol{b}) < \chi^2_{max}(\boldsymbol{b}_0)$, then the current value of b_1 is within the uncertainty interval. Conversely, if $\chi^2_{min}(\boldsymbol{b}) > \chi^2_{max}(\boldsymbol{b}_0)$, then the current value of b_1 is rejected by the data. (Note that this simple formula is adequate when a continuous uncertainty interval is well-centered on the maximum likelihood solution. A slightly more complicated scenario will be considered in Section IV.)
7- The analysis is iteratively repeated from Step 3 until the limits of the uncertainty interval are located to the desired degree of resolution.

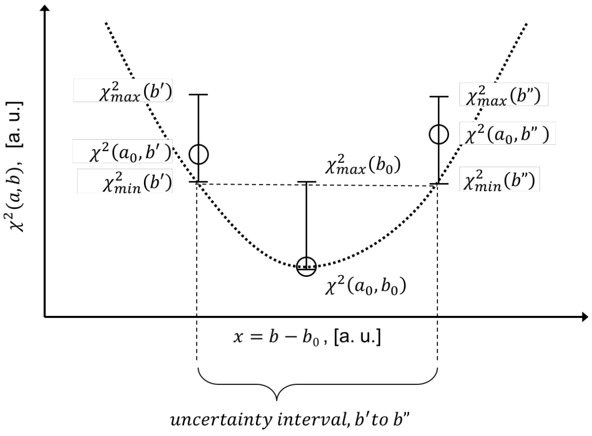

Figure 2. *Illustration of inference of the uncertainty interval in the optimizable variable of interest,* b. *The maximum likelihood solution corresponds to the least-squares solution obtained at point* (a_0, b_0). *The maximum value of* χ^2 *at* b_0 *is obtained for an extremum of the model parameter* a. *For all other points along the principle axis* $x=b-b_0$, *the minimum value of* χ^2 *is obtained by re-optimizing all other parameters, including a (within the bounds of its prior probability distribution). Locations along the ordinate axis where a value of* χ^2 *less than* $\chi^2_{max}(b_0)$ *cannot be obtained lie outside the uncertainty interval. The dashed curve shown represents a principle curve of the surface* $\chi^2(a,b)$.

The implementation of model parameter priors as error bars on a least-squares fitting error metric may be compared to the Bayesian approach of multiplying these priors by the likelihood to produce a posterior probability. In the former analysis, one evaluates a χ^2 that is akin to the quantity $-Log[P(d|\boldsymbol{b})]$, where d is the image data and the prior probability distribution for $\boldsymbol{b}$ is unity everywhere and omitted from the analysis. One then adds (or subtracts, if appropriate) a value due to the propagation of prior information about the additional parameters, $\boldsymbol{a}$. So long as $P(\boldsymbol{a})$ is a simple function, it is straightforward to demonstrate the equivalence to the posterior likelihood, $P(d|\boldsymbol{b},\boldsymbol{a}) * P(\boldsymbol{a})$. When more sophisticated prior information is available, i.e. $P(\boldsymbol{a})$ is not rectangular, more sophisticated analysis, e.g. direct evaluation of the posterior probability, may be required. However, for the given task, one may consider this method of generating an uncertainty interval as equivalent to defining a contiguous range in a given parameter b_k over which equal values of the posterior probability are available: the uncertainty interval corresponds to the contiguous region in the space $(\boldsymbol{a},\boldsymbol{b})$ where equivalent values of $-Log[P(d|\boldsymbol{b},\boldsymbol{a}) * P(\boldsymbol{a})]$ exist. A single, most probable solution, $(\boldsymbol{a_0},\boldsymbol{b_0})$, may exist within this interval, but one must keep in mind that they are not free to solve for $\boldsymbol{a}_0$. Rather, one must consider all possible values of $\boldsymbol{a}$.

The presence of systematic errors can reduce the quality of inferences made from the above analysis. If, as in the ideal case, one may assume that there are no systematic errors present, and that random errors contribute a constant error in least-squares analysis, then uncertainty analysis is simplified to the point that it can be performed without returning to the data simply by evaluating the behavior of the forward model, i.e. $\sum_{i=1}^{N}[M_i(\boldsymbol{a},\boldsymbol{b}) - M_i(\boldsymbol{a_0},\boldsymbol{b_0})]^2$. In this scenario, it becomes possible to make rather definitive statements about the sources of uncertainty in the experiment, even make prescriptions for improving the measurement. However, when systematic errors are present in the analysis due to inadequacies of the forward model in representing the experiment, it is no longer possible to ascertain the source of the uncertainty. The error metric, χ^2, no longer varies in a predictable manner. In other words, systematic errors are accounted for in the analysis described above, but not resolved. This must be appreciated when interpreting the results obtained in the example problem of Section IV.

Inspection of the spatially varying residual data, $\chi_{x,y} - \left[M_{x,y}(\boldsymbol{a},\boldsymbol{b}) - M_{x,y}(\boldsymbol{a_0},\boldsymbol{b_0})\right]$, shown in Figure 3 (c), reveals that it is comprised of three main components: a uniformly distributed noise with high spatial frequency and weak spatial correlations, a vertically oriented striation of the gain and background scattered fields, and a systematic warping of the image that makes some regions easier than others to align with the model. The last two artifacts are most likely a result of the scanning method used for these storage-phosphor image plates. The systematic errors (striation and warping) are minimized by optimizing the orientation of the image and a fitting a parameterized spatially varying background scatter field. It must be acknowledged that systematic error contributions are probably not constant versus variation of the model parameters or quantities of interest. Therefore, they probably do not make for a perfectly constant contribution to χ^2 in this analysis. This effect, in general, increases the uncertainty of the analysis, widening the uncertainty interval. It is only in that their contribution appears to remain small compared to the modeled error and random error terms that one may proceed to obtain quantitative estimates for the parameters of interest.

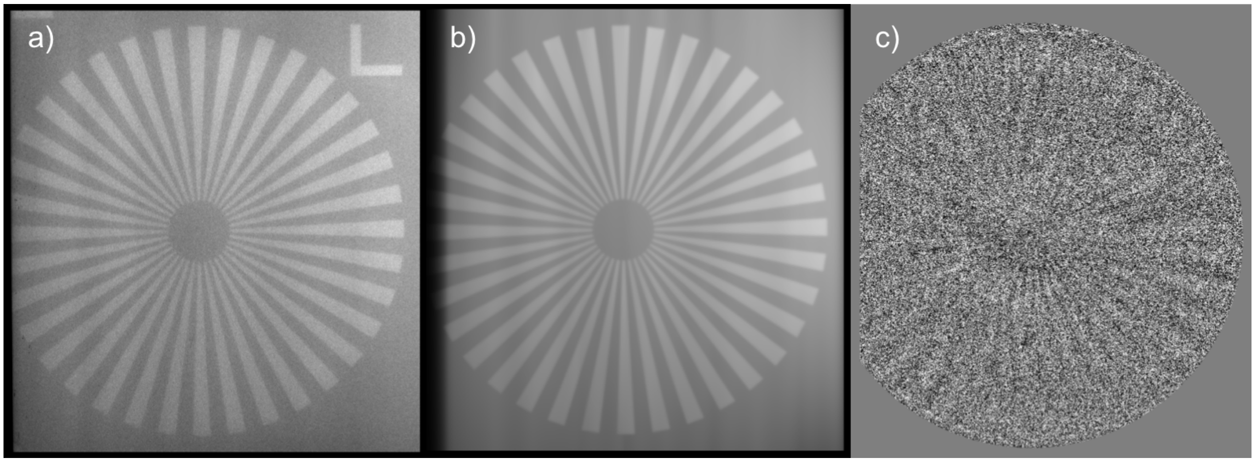

Figure 3. *The radiographic image (a), forward model (b), and spatially varying residuals image (c) obtained from analysis of an image plate from TRIDENT laser discharge #26251 (radiographic magnification of approximately 3.1). Inspection of this image suggests that the residual error is dominated by uncorrelated, random noise with high spatial frequency.*

IV. ANALYSIS OF LASER-DRIVEN RADIOGRAPHY EXPERIMENTS AT THE TRIDENT LASER FACILITY

A common method of generating high-energy photons for the inspection of 2D and 3D objects is the acceleration of a magnetically-focused relativistic electron beam [Ekdahl 2002] into a target of heavy ions where x-rays are produced by bremsstrahlung, or the braking of the electrons by collisions with an electron-photon converter target [Schiff 1951, Koch and Motz 1959]. The photon spectrum and radiographic spot size are manipulated by varying the electron energy spectrum, beam focusing, and converter target properties. In laser-driven radiography, a high intensity laser pulse is used to accelerate electrons into a plasma or a high-Z solid target [Perry 1997, Edwards 2002, Glinec 2005, Courtois 2009, Courtois 2011, Compant 2012, Nakamura 2012, Nerush 2014]. This may have several advantages over the use of conventional electron beam acceleration schemes. For one, laser energy can be transmitted over large distances and relayed into the radiographic setup at arbitrary angles, allowing greater flexibility in the arrangement of an experiment for a given facility. Laser technology also continues to advance rapidly, which may allow for much more compact designs in the near future. And of great importance for radiographic resolution, space charge effects do not limit the intensity of laser energy deposition. Laser-driven radiography can therefore, in many regimes, produce smaller radiographic spot sizes than are possible with conventional electron beam accelerators [Edwards 2002, Cortois 2011, Cortois 2013].

Laser-driven radiography experiments were carried out in order to explore the physics and potential benefits of features unique to the TRIDENT laser facility. TRIDENT is a 30 TW, high-contrast laser capable of delivering more than 70 J at intensities greater than 10^{20} W/cm^2 [Moncur 1995]. Furthermore, pioneering work at TRIDENT has furthered the development of electron and ion acceleration techniques using thin metallic foil laser targets [Hegelich 2006, Fuchs 2005, Cowan 2004]. For the study presented here, BIE analysis is used to infer the radiographic spot size for both thick target (1 mm Ta) and thin-foil (~100 nm Al) laser-driven radiography techniques.

Analysis of the data to infer radiographic spot size, or source blur, is dependent upon determination of the detector blur function. For shot #26262, shown in Figure 4, the laser energy was deposited on a 110 nm, optically flat, Al foil so as to accelerate relativistic electrons toward a 1 mm thick Ta converter target, the radiographic photon source, approximately 250 μm downstream. As a detector, three phosphor image plates are stacked between four 30 mil sheets of Ta. As mentioned earlier, limiting resolution as high as 5.9 lp/mm has been achieved by a similar arrangement. The 10 cm x 10 cm resolution target plate was placed in direct contact with the first Ta intensifier sheet such that all blur in the image may be attributed, to a good approximation, to blur inherent to the detector. Analysis using the BIE determined maximum likelihood solutions for detector resolution at the three image plates in the range of 0.3 to 0.4 lp/mm. This is the range that was subsequently used in uncertainty analysis for inference of the source blur, or radiographic spot size.

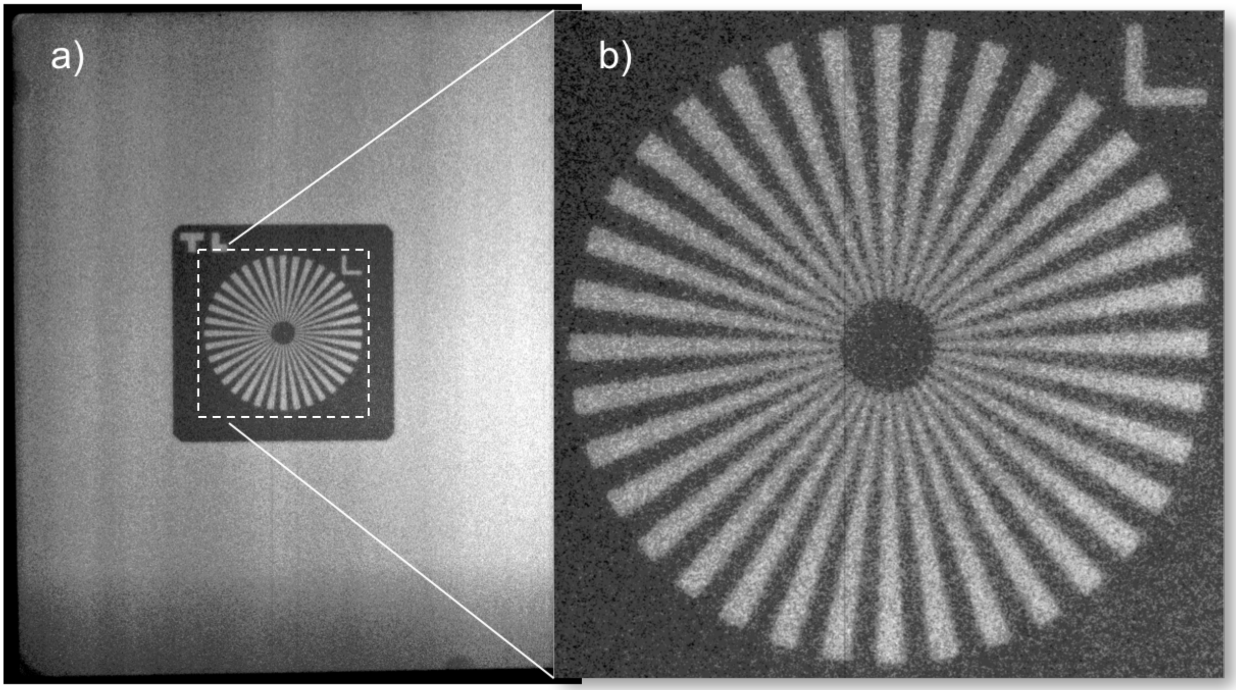

Figure 4. *(a) An image of the full 40 x 35 cm phosphor image plate, and (b) an enlargement of the region of interest where the R2DTO resolution target is in contact with the image plate stack. The image shown is taken from the 3rd downstream plate, plate C, at 100 μm resolution. The radiographic magnification is 1:1.*

Note that in Figure 4 (a) there appears to be a large degree of spatial variation in the contrast, or gain of the image, as well as the apparent background scatter field. These will ultimately be represented in the BIE as fitted additive and multiplicative fields with a large number of free parameters. However, by restricting the spatial frequency of these fields to be much lower than that of the detector and source blur kernels, competition between the two is effectively eliminated. The parameters describing additive and multiplicative fields bear no covariance with the source spot size in terms of their effect on χ^2.

After having established an error bar (or equivalently, a uniform prior probability distribution function) for the detector blur kernel, radiographic imaging at a radiographic magnification of 6.2 is analyzed. At this magnification, blur is well-resolved by the 100 μm resolution image plate; BIE analysis is performed at an interpolated resolution of 15 μm in the resolution target, or object, plane. Figure 5 provides an example of the image data produced during shot #26270, along with the forward model produced by the BIE and residual data resulting from comparison of forward modeling and experimental results. In this shot, x-ray photons are produced by depositing laser energy on a relatively thick target (1 mm Ta) to generate free electrons, accelerating them by a combination of ponderomotive and wakefield acceleration mechanisms [Tajima and Dawson, 1979] and converting them by bremsstrahlung in the same material.

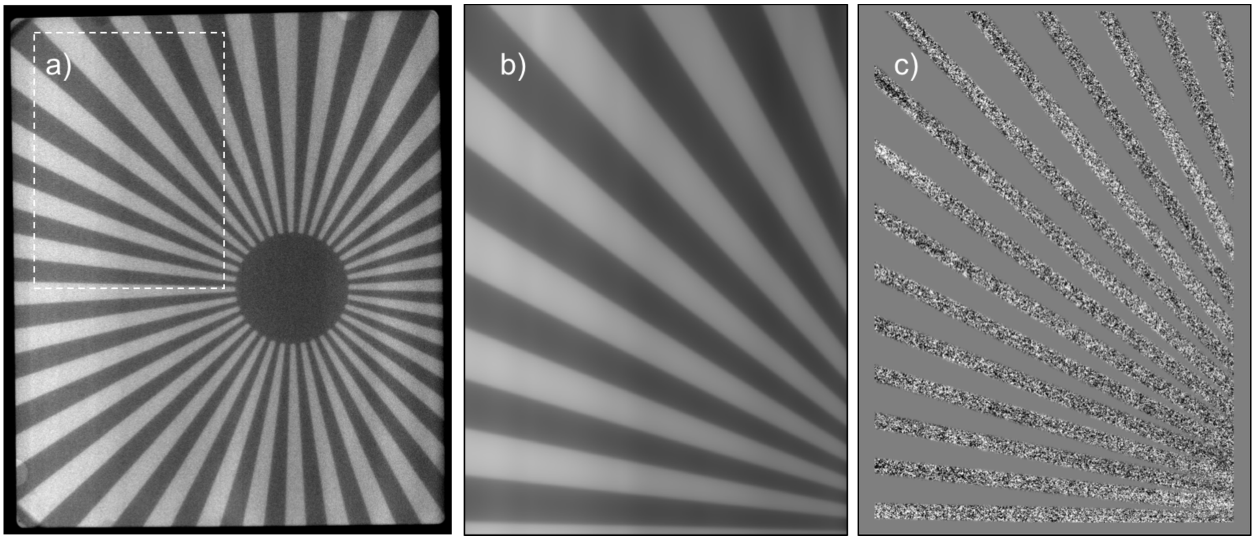

Figure 5. *(a) Data from the phosphor image plate exposed during shot #26270 with a radiographic magnification of approximately 6.2. (b) The forward modeled image data from the region of interest (dashed square in (a)) produced by the BIE. (c) Residual data obtained by subtracting image (b) from image (a). A residual mask, or weighting function, is applied to isolate resolution target edges in the contribution to* χ^2.

The algorithm described in Section III is applied to obtain the data shown in Figure 6. Both the minimum and maximum values of χ^2 that may be obtained within the range of possible detector blur functions are shown where relevant. The blue triangles represent data that is obtained at the maximum value of detector blur, a detector resolving power of 0.3 lp/mm. For large values of source blur, these points produce large values of χ^2. Conversely, at sufficiently small values of source blur, smaller radiographic spot sizes, these points constitute the minimum available χ^2. This trade-off between source and detector blur persists for the minimum value of detector blur, a resolving power of 0.4 lp/mm (red diamonds). Green circles indicate points within the uncertainty interval where the detector blur has been optimized for the given source blur. The point in the middle of the plot where curves fitting these two sets of points would intersect identifies the upper bound on relevant values of χ^2, a value that defines the uncertainty interval. Points lying below this are within the interval, which spans approximately 35 to 170 μm in Figure 6, part (a). This range of radiographic spot sizes is consistent with expectations developed from a survey of published results.

Note the trend in χ^2 that is apparent in the vicinity of the maximum likelihood solution in Figure 6, part (a). This is not due to systematic errors, but rather an effect that can be understood in terms of the features of the model. This is illustrated in Figure 6, part (b), where the *model error* term of Section II is evaluated off-line by comparing the modeled maximum likelihood solution to other models with other radiographic spot sizes. The χ^2 at left (blue triangle) is zero, and variation as a function of spot size FWHM reproduces the behavior observed in part (a). The trend is attributed to the difference between the functional form of the phosphor image blur kernel and the source blur kernel. The former is defined as the Fourier transform of the following function:

$$Q \equiv \left[\left(\frac{C}{\alpha}\right)^2 + 1\right]^{-1}, \tag{4}$$

where C is a normalizing constant and α is proportional to the spatial cutoff frequency in inverse mm. For Figure 6, the source blur kernel is taken to be a symmetric 2D Bennett function [Bennett 1934],

$$f(x,y) = \left(1 + \left[\frac{(x_0 - x)}{a_x}\right]^2 + \left[\frac{(y_0 - y)}{a_y}\right]^2\right)^{-2}, \tag{5}$$

where the distribution is centered at $(x_0 = 0, y_0 = 0)$ and $a_x = a_y$.

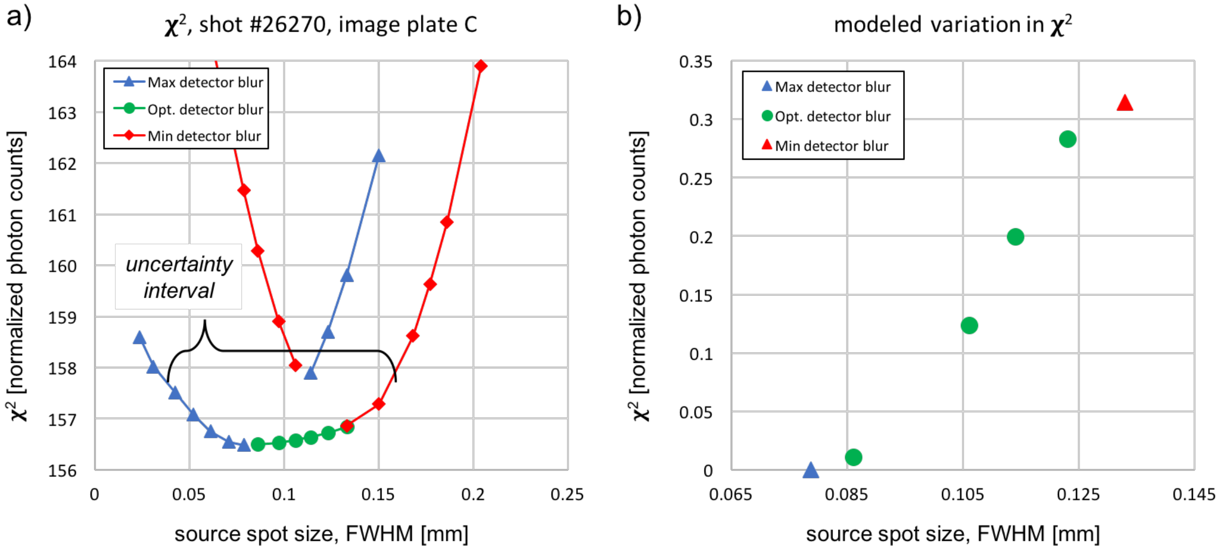

Figure 6. *(a) Analysis of χ^2 as a function of the source spot size, FWHM, for shot #26270 using a symmetric Bennett function distribution. The uncertainty interval is indicated, spanning approximately 35 to 170 µm. (b) The error that may be induced by comparing the forward-modeled maximum likelihood solution to forward models with different source spot sizes. The variation in this so-called* modeled error *accounts for variations in χ^2 observed in (a), lending credence to the assertion that random and systematic errors do not have a significant impact on the behavior of χ^2 in this region.*

In the analysis presented here, the functional form of the source blur kernel is chosen independently and for each evaluation of the source blur uncertainty interval. There is no external information presented here that dictates preference for one functional form or another, and, in principle, it could be parameterized and optimized along with all other optimizable variables, b_k. It is strictly for convenience that this work focuses on only two functional forms: the Bennett distribution and an exponential form. The exponential form, defined by the radial point-spread function,

$$PSF(r) = a\pi f_c e^{-2\pi f_c r}, \tag{6}$$

where a is a normalizing constant and f_c is the spatial cutoff frequency, is used to produce the data shown in Figure 7. Note that the behavior of χ^2 has changed. The minimum values of χ^2 are slightly lower, the trend near the maximum likelihood solution seen in Figure 6 is much less prominent, and the entire uncertainty interval has shifted toward larger spot sizes.

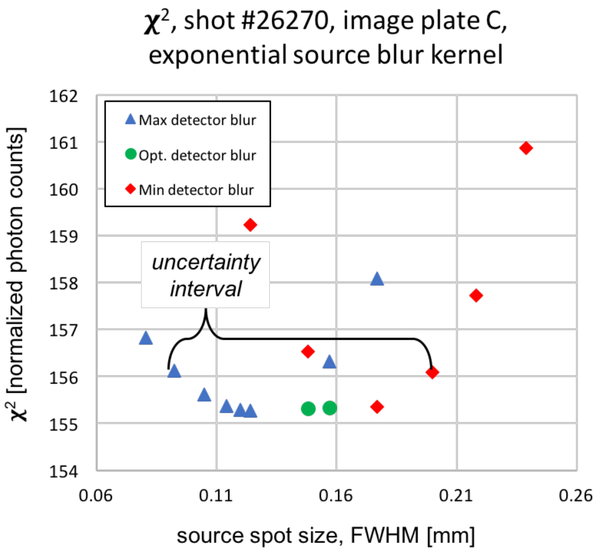

Figure 7. *The behavior of χ^2 vs. spot size FWHM is evaluated for shot #26270 using an exponential source blur kernel. The upper bound of this uncertainty interval is approximately 195 µm.*

The images shown earlier in Figure 3 were obtained with a radiographic magnification of approximately 3.1. For that shot, #26251, the laser energy was deposited on a 110 nm Al foil set approximately 250 µm upstream from a 1 mm thick Ta converter target. The analysis of the third phosphor image plate in the detector pack, plate C, is shown in Figure 8. In part (a), a symmetric 2D Bennett source blur kernel is used. In part (b), the blur kernel is a radial exponential point spread function. In both cases, the inferred spot size is much larger than in the case of the single, thick laser target (Figures 5, 6, and 7). Note that the fitting error is smaller when the model employs a Bennett distribution (FWHM 270-520 µm), which is opposite the results from the thick target case, shot #26270, where the exponential source blur kernel yielded better fits to the data. This implies that the shape of the spot may also be different.

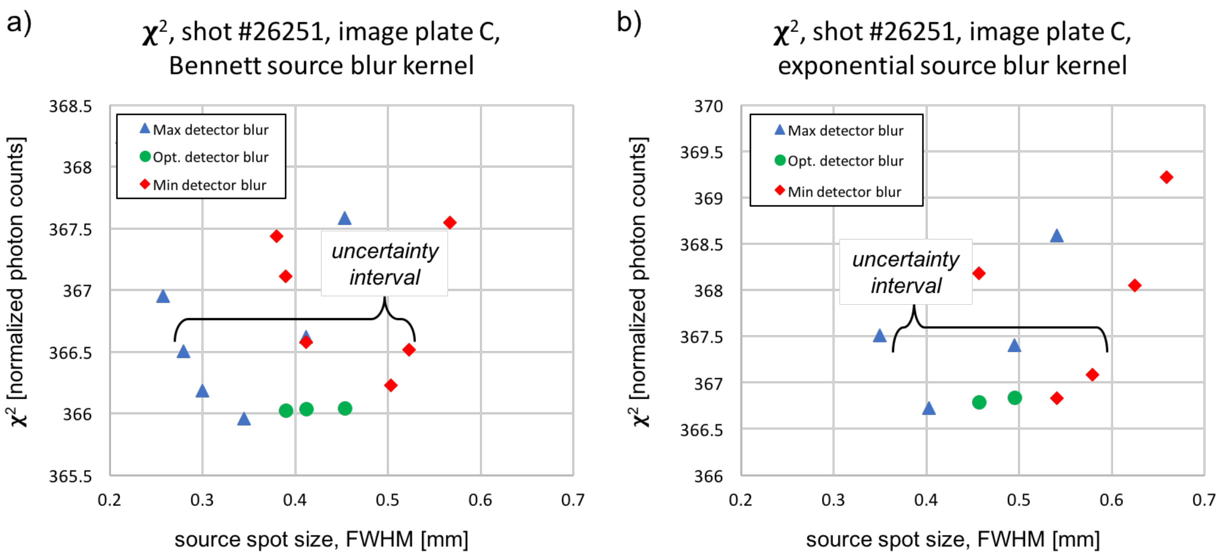

Figure 8. *(a) Analysis of χ^2 vs. source spot size for shot #26251, radiographic magnification of approximately 3.1, using a Bennett function blur kernel. (b) The same, but using an exponential source blur kernel. The combined range of uncertainty is approximately 270-600 μm, FWHM.*

There are other meaningful differences between the data obtained for the thick and thin laser targets in this experiment. For shot #262651, the resolution in the resolution target (object) plane is interpolated to 30 μm (vs. 15 μm in shot #262670), and a larger region of the phosphor image plate is used for the analysis. This exacerbates issues with the alignment of a warped image to the ideal geometry of the BIE forward model. However, these differences are unable to account for the large increase in the inferred spot size. The mean values within the uncertainty intervals inferred for Bennett and exponential source blur kernels are roughly a factor of 4 larger than for the thick laser target. Values in the range of 100-200 μm, consistent with the results for thick target laser-driven radiography, are certainly excluded by the data in that case. And this discrepancy is only exaggerated by the fact that very favorable prior information about the detector source blur has been applied. The data obtained during this experiment provided estimates of detector resolution in the range of 0.3 to 0.4 lp/mm. If an assumption of higher resolution is applied, then much larger radiographic spot sizes are inferred by this analysis.

V. DISCUSSION

Random errors resulting from stochastic processes, i.e. noise, do not increase uncertainty in the inference of the most likely value of a parameter of interest except when the analysis is predominantly impacted by a small number of data points or a subset of pixels within an image. This can be understood by contrasting the least-squares optimization approach and the associated choice of definition for χ^2 with the method of maximum likelihood, where the weighting of χ^2 due to random, stochastic processes is pre-defined in terms of a pre-determined probability distribution function [Bevington 1969]. Identifying the optimal parameters is reduced to optimizing the chosen probability distribution function when the parameterized model is substituted for the unknown parent distribution. For common probability distribution functions, the term that is to be minimized includes the variance of the data as a normalizing coefficient. For example, if one maximizes the Gaussian probability distribution,

$$P(x) \propto e^{-\Sigma\left(\frac{x-y}{\sqrt{2}\sigma}\right)^2}, \tag{7}$$

this corresponds to minimizing a weighted χ^2 function,

$$\chi^2 \equiv \Sigma\left(\frac{x-y}{\sqrt{2}\sigma}\right)^2. \tag{8}$$

In comparison with the earlier formulation for a simple least-squares optimization scheme, the derivative of χ^2 in any direction is inversely proportional to the noise level. For $2\sigma^2 > 1$, this can reduce the curvature about the maximum likelihood solution. However, one should not rush to assume that this would increase the uncertainty interval, or even makes the result dependent on the noise level. In fact, the analysis presented in this paper is already equivalent to the maximum likelihood approach when applying a uniform weighting coefficient. One may still use the resultant directional derivatives to resolve the uncertainty in an independent variable, Δa, from the corresponding variation of the imaging data, Δd, obtained from a random sampling of images by using an equation of the form,

$$\Delta d \simeq \sum_i \Delta a_i \left(\frac{\partial d}{\partial a_i}\right). \tag{9}$$

It is worth noting, however, that χ^2 must be defined in a manner that includes the normalizing coefficient taken from the appropriate probability distribution function if it is to be taken as the posterior probability of the solution through inverse-logarithmic transformation.

Systematic errors include all processes that are not both random and stochastic, including artifacts in the data that might, without quantitative analysis of their properties, be casually referred to as noise. Systematic errors are not properly represented by the forward modeling of the experiment. They may exhibit correlated behavior with the parameters that are included in the model, modifying the behavior of the error metric around the optimized least-squares solution. This increases uncertainty and rigorously encapsulates the intuitive principle that the certainty of inference by analysis of experimental data is directly related to the quality of the forward model available for replicating experimental conditions, properly representing physical processes utilized by the instrumentation, and producing synthetic diagnostic data.

Reduction of systematic errors, a topic beyond the scope of this paper, is facilitated by the framework described here. An offline evaluation of the behavior of contributions to the error metric that can be accounted for by the forward model is possible in most cases and allows for an algebraic isolation of systematic effects. When it is possible to establish that systematic errors are either constant or insignificant, it may be said that they do not impact the uncertainty interval about the maximum likelihood solution. Conversely, when they are significant, quantification of their impact may yield important insights as to what aspects of the forward modeling technique must be improved.

A distinction between *model parameters* and *optimizable variables* within the forward model is essential for determining the *uncertainty interval*. The prior probability distribution function associated with a *model parameter* generates an error bar on the χ^2 obtained in subsequent analysis. This obviates the need for improving prior information about these parameters. Furthermore, it motivates one to investigate the propagation of the prior distribution as an error throughout the forward model so as to prioritize external investigations according to those parameters that generate the greatest errors. With regard to *optimizable variables*, it is straight-forward to deduce that one should endeavor to reduce the number of these free parameters to a single quantity of interest. Any additional variables that can be freely optimized will tend to reduce the χ^2 at locations away from the maximum likelihood solution, i.e. reduce the curvature along the principle axis of interest, and increase the uncertainty interval. Where possible, *optimizable variables* such as those describing detector gain or the form of the background scatter field should be replaced with physics-based models and assigned the most stringent priors possible. This ensures that variation of the *optimization parameter of interest* has the greatest possible impact on χ^2 and cannot be compensated for by arbitrary re-optimizations of other variables within the forward model.

VI. REFERENCES

Bennett, W.H., Physical Review **45**, pp. 890-897 (1934).

Bevington, P.R., *Data Reduction and Error Analysis for the Physical Sciences*, McGraw-Hill, New York, 1969.

International Bureau of Weights and Measures (BIPM), *International vocabulary of metrology – Basic and general concepts and associated terms (VIM)*, 3rd ed., 2008.

Bode, H.W., *Network Analysis and Feedback Amplifier Design*, Van Nostrand, Princeton, NJ, 1945

Compant La Fontaine, A., Physics of Plasmas **19**, 023104 (2012)

Courtois, C., et al., Physics of Plasmas **16**, 013105 (2009)

Courtois, C., et al., Physics of Plasmas **18**, 023101 (2012)

Courtois, C., et al., Physics of Plasmas **20**, 083114 (2013)

Cowan, G., *Statistical Data Analysis*, Dowden, Hutchinson and Ross, Stroudsburg, PA, 1973.

Cowan, T.E., et al., Physical Review Letters **92**, 204801 (2004)

Disterhaupt, J.L.S., *Quantifying the Performance of Blur Calibration Targets Used at DARHT*, LA-CP-15-20567, 2015.

Edwards, R.D., Applied Physics Letters **80**, 2129 (2002)

Ekdahl, C., IEEE Transactions on Plasma Science **30**, pp. 254-261 (2002)

Fuchs, J., et al., Physical Review Letters **94**, 045004 (2005)

Glinec, Y., et al., Physical Review Letters **94**, 025003 (2005)

Hanson, K.M., *Medical Imaging: Image Processing*, pp. 716-731 (1993)

Hanson, K.M. and Cunningham, G.S., *Medical Imaging 1996: Image Processing*, pp. 416-436 (1995)

Hanson, K.M. and Cunningham, G.S., *Maximum Entropy and Bayesian Methods*, pp. 125-134 (1996).

Hegelich, B.M., et al., Nature **439**, 441-444 (2006)

Koch, H.W. and Motz, J.W., Reviews of Modern Physics **31**, 920 (1959)

Laplace, P.S., Memoir on the Probability of the Causes of Events, Memoires of Mathematics and Physics **6**, pp. 621-656 (1774).

Laplace, P.S., *A Philosophical Essay on Probabilities*, 1814.

Moncur, N.K., et al., Applied Optics **34**, pp. 4274-4283 (1995)

Myers, R.H., *Response Surface Methodology*, Allyn and Bacon, Boston, MA, 1971.

Nakamura, T., et al., Physical Review Letters **108**, 195001 (2012)

Nerush, E.N., et al., Physics of Plasmas **21**, 013109 (2014)

Perry, M.D., et al., *Laser Driven Radiography*, UCRL-ID-129314 (1997)

Rabinovich, S.G., *Measurement Errors and Uncertainties: Theory and Practice,* 2nd ed., Springer-Verlag, New York, NY, 2000.

Ronen, Y., *Uncertainty Analysis*, Franklin, 1988.

Sayag, M. “Light stimulating and collecting methods and apparatus for storage-phosphor image plates.” U.S. Patent No 6,800,870. 5 Oct. 2004.

Schiff, L.I., Physical Review **83**, 252 (1951)

Seely, J.F., Applied Optics **47**, pp. 5753-5761 (2008)

Shapiro, S.S., and Gross, A.J., *Statistical modeling techniques*, Dekker, New York, NY 1981.

Tajima, T. and Dawson, J.M., Physical Review Letters **43**, pp. 267-270 (1979)

Wigner, E.P., Effect of small perturbations on pile period, Manhattan Project Report CP-G-3048, 1945.